Polym. Bull. (2015) 72:1–17
DOI 10.1007/s00289-014-1255-6

ORIGINAL PAPER

Synthesis and characterization of polyurethane–organoclay nanocomposites based on renewable castor oil polyols

M. A. Alaa · Kamal Yusoh · S. F. Hasany

Received: 6 January 2014 / Revised: 20 July 2014 / Accepted: 21 September 2014 /
Published online: 1 October 2014

Abstract In this study, castor oil-based polyurethanes–organoclay (COPUs-Cloisite 30B) nanocomposites are synthesized by mixing polypropylene glycol polyol and dehydrated castor oil (15 %), enforced with C30B nanofillers, at different weight percentages. The physico-chemical behaviors were evaluated by Fourier transform infrared spectroscopy, Fourier scanning electron microscopy, scanning electron microscopy and X-ray diffraction. Thermal stability was found improved up to ~30 °C in the sample with 5 wt% of C30B. Tensile properties depicted an improvement of ~240 % in tensile strength and decrease of ~30 % in elongation with 5 wt% organoclay, respectively. Improved physico-chemical properties of COPUs-C30B signify the usage of COPUs-C30B in the industrial and commercial applications, i.e. coatings, adhesives and automotive applications.

Keywords Renewable polyols · Polypropylene glycol polyol · Castor oil · Cloisite 30B · Physico-chemical behaviors

Introduction

Polyurethanes (PUs) with distinctive physical and chemical properties are flexible, high mechanical, thermal [1–3] and chemical resistance polymers. PUs can be tailored to meet diversified demands of various applications such as rigid insulations, coatings, footwear adhesives [4], fibers, thermoplastic elastomers,

M. A. Alaa (✉) · K. Yusoh · S. F. Hasany
Faculty of Chemical and Natural Resources Engineering, University Malaysia Pahang, 26300 Kuantan, Malaysia
e-mail: allavip63@yahoo.com

M. A. Alaa
Department of Chemical Engineering, University of Technology, Baghdad, Iraq

foams as well as medical devices [5–7]. A great demand of renewable resources for polyurethane (PU) synthesis, leads a pathway to the new environmental-friendly polymers, with low cost, controlled life span, and both good physical and biodegradable characteristics [8, 9]. Polyols from vegetable oils [10, 11], such as soybean [12, 13] castor [14, 15], canola [16, 17], and palm [18, 19] oils are increasingly being regarded as a sustainable alternate to the mainstream hydrocarbon-based feedstocks. These oils are cost-competitive and are environment-friendly. Castor oil exhibits an unusual chemical composition that makes it quite valuable for many applications especially in the production of polyurethanes by reacting with different diisocyanates [20]. It also presents advantages such as: renewability, non-edible, easy availability in a large quantities, and low cost over other vegetable oils [21, 22], with some drawbacks like low thermal stability and mechanical strength [23, 24].

A great deal of work has been devoted to the development of the polyurethane structure; morphology and properties by introducing new chemical structures in the backbone chains [25], in order to increase the structural integrity of the polyurethane matrix or by strengthening with various organic or inorganic fillers within continuous polymer matrix. In recent years, lots of research efforts have been undertaken on layered silicate [26, 27] filled polymer nanocomposites as this kind of material may exhibit drastic improvements of thermal, mechanical and physico-chemical properties compared to the neat polymer. Number of research works has been reported related to the castor oil-based polyurethane–organoclay nanocomposites, depending upon type and ratios of diisocyanates, chain extenders and weight percentages of organoclay [28]. Kaushik et al. [29] studied a series of 1,4-butane diol chain extended polyurethane nanocomposites based on castor oil, 4,4-diphenylmethane diisocyanate (MDI) with modified clay (Cloisite 30B) as a filler. These nanocomposites exhibited lower water absorption and diffusivity values as compared to neat polyurethane and thermal stability improved with increased percentage of organoclay. Krushna and Nayak [30] investigated the synthesis of polyurethane nanocomposites prepared from natural oil like castor oil using HMDI and organically modified clay and covalently linked PU/n-HMDI composite, which was later collected successfully by the electro spinning process. Swagatika et al. [31] investigated polyurethane/montmorillonite nanocomposites from castor oil, synthesized with organically modified layered-silicates (organoclays) by in situ polymerization. The results showed a higher improvement of tensile modulus in the polyurethane/montmorillonite nanocomposites can be attributed when the better dispersion and intercalation/exfoliation of the nanoparticles in a polymer matrix. dos Santos et al. [32] observed increased mechanical performance in proportion to contend of diisocyanate.

The aim of this study is to develop environmental friendly and economical PUs nanocomposites based on a mixture of (polypropylene glycol polyol and dehydrated castor oil 15 %) via in situ polymerization, which up to this date has not been reported. Organoclay (Cloisite 30B) was used as a nanofiller at different weight percentages up to 5 % loading, to study the variation in physical and chemical properties.

Experimental

Materials

The organoclays were purchased from Southern Clay Products Inc., USA. The modifiers for organoclay (Cloisite 30B) were dehydrogenated tallow quaternary methyl tallow bis-2-hydroxyethyl quaternary ammonium (MT2EtOT). The modifier concentration for C30B was 95 mequiv./100 g clay and 90 mequiv./100 g clay. Castor oil was commercial grade and was purchased from the local market. It was dehydrated at 80 °C in a vacuum oven and characterized for hydroxyl value (164.5), acid value (3) and moisture content (0.379 %), to avoid any moisture presence in a closed (controlled oxygen) synthesis; to limit any side reactions, changes in chemical behavior, and to avoid air bubbles in the finished films. Polypropylene glycol (PPG) (Mn = 4,000) was supplied by Sigma-Aldrich Company. Chain extender, 1,4-butane diol was procured from Himedia, India. The toluene diisocyanate (TDI) which was used as received was supplied from Sigma-Aldrich Company.

Synthesis mechanism

Synthesis mechanism of COPUs-organoclay (Cloisite 30B) nanocomposites by in situ polymerization method as shown in (Fig. 1) encompass two major steps. Firstly organoclay gets dispersed in polyols mixture (PPG + 15 % castor oil), while in the second step dispersed organoclay in polyols mixture reacted with isocyanate groups to produce a castor oil-based pre-polymer, followed by a reaction with chain extender (diol) in the presence of a catalyst to produce COPUs-C30B nanocomposites.

Synthesis of polyurethane–organoclay (COPUs-C30B) nanocomposites

The COPUs-C30B nanocomposite was prepared by in situ polymerization technique. Firstly, different organoclay concentrations (0, 1, 3 and 5 wt%) were prepared by blending the organoclay in polypropylene glycol polyol and dehydrated castor oil (15 %) at 80 °C and with sonication time ranges from 1 to 5 h (60 °C, 9 kHz). The mixtures were degassed under nitrogen atmosphere for 20 min. In the second step, 100 g of already blended mixture was added with 15.5 g of toluene diisocyanate (TDI) in small portions and vacuum degassed for 3–5 min to achieve homogenous reaction conditions by preventing bubbles. Pre-polymer obtained in the last step, was finally reacted with 2.25 g of 1,4-butanediol and 0.6 g catalyst (DABCO) for quick aggregation of about 2 min, till the viscous mixture appeared. The mixture was poured into a glass petridish and thin film of approximate thickness (0.8–1.0 mm) was obtained, while curing at 50 °C for 24 h. The obtained sample was post-cured for a week time at 80 °C.

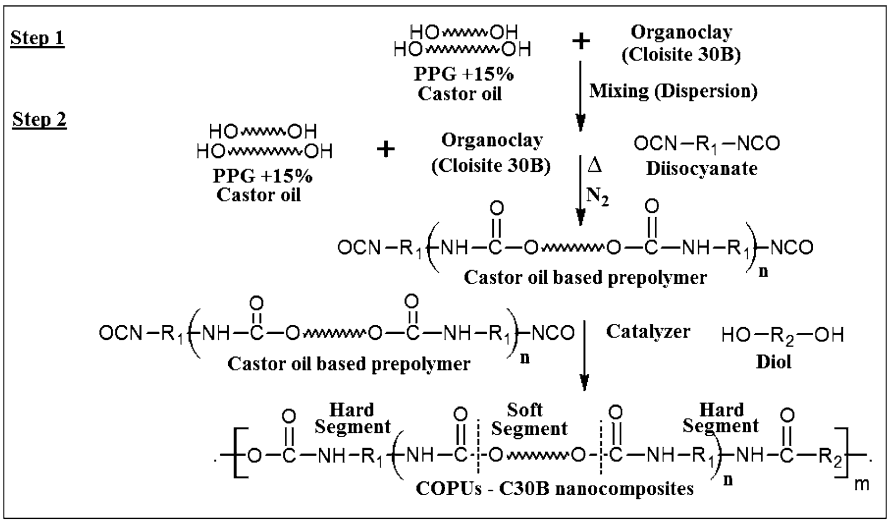

Fig. 1 Schematics representation of synthesis mechanism of (COPUs-C30B) nanocomposites with in situ polymerization method

Characterization

The prepared COPUs-C30B nanocomposites were characterized by Fourier transform infrared spectroscopy (FTIR) analysis of COPUs-C30B nanocomposites was done using a FTIR spectrometer (Nicolet 5DX FTIR, USA). A wide-angle X-ray diffraction (WAXD) was used with X-ray diffractometer (Rigaku Mini Flex II, Japan) employing a graphite monochromator and CuKa radiation (l 0.15406 nm). The morphology of the nanocomposites was examined by field emission scanning electron microscopy (FESEM; JEOL EVO-50, Japan) and scanning electron microscopy (SEM; JEOL 6300F, Japan) at an acceleration voltage of 5 kV. Thermal stability of polyurethane nanocomposites was determined using a thermogravimetric analyzer (TGA) of type thermogravimetric analysis (TGA) experiments were carried out using a Universal V4.5A, TA Instruments under a nitrogen atmosphere. Tensile testing of the nanocomposites was carried out on an Instron model 4505 universal testing machine at 25 °C, with a load cell of 5 KN and following ASTM D 638. The crosshead speed was set to 2 mm/min. Samples were cut in a dumbbell shape with an ASTM D 638 (type V).

Results and discussion

FTIR of polyurethane nanocomposites

Figure 2 depicted a comparative FTIR spectrum of organoclay (Cloisite 30B) with neat COPUs, while in Fig. 3 relative FTIR spectra of neat COPUs with different wt% of (COPUs-C30B) nanocomposites are studied. Organoclays derived from

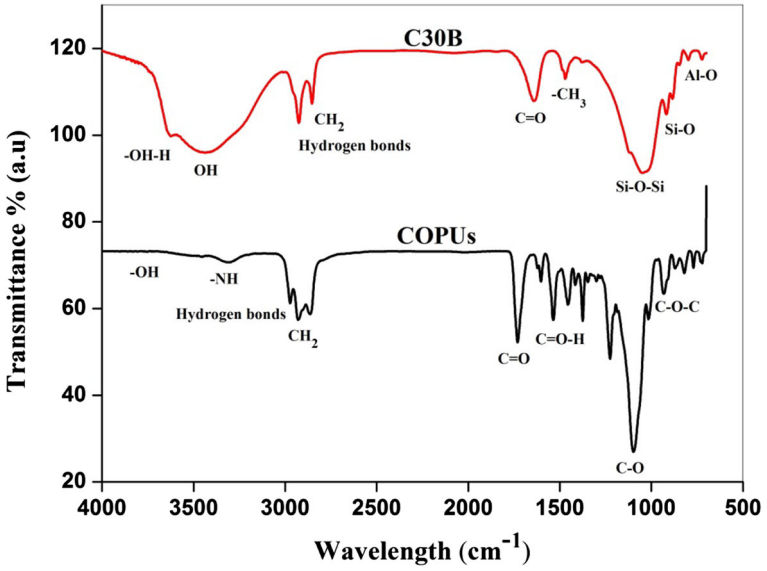

Fig. 2 FTIR spectra of organoclay (C30B) and COPUs

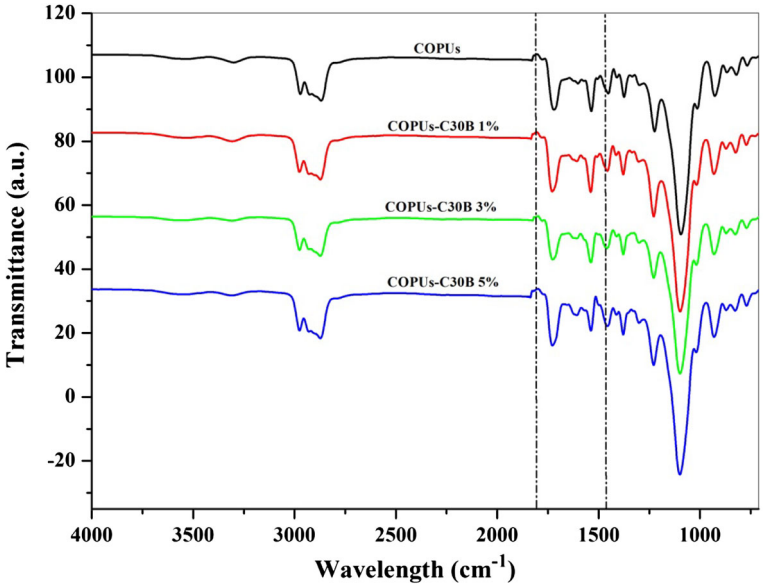

Fig. 3 FTIR spectra of COPUs and (COPUs-C30B) nanocomposite with different percentages of organoclays

montmorillonite (MMT) with the specific peaks of organoclay, the characteristic absorptions peaks of the organoclay at 1,050 cm^{-1} which are similar to stretching vibrations of Si–O–Si, 525 and 460 cm^{-1} correspond to Al–O and Si–O bending

vibrations, respectively [32]. The absorption bands at 3,550 and 3,395 cm^{-1} are ascribed to the free –OH stretching and the hydrogen-bonded –OH stretching, respectively.

The 1,655 cm^{-1} band for organoclay is caused by the hydrogen free carbonyl, and the bands at 1,455 and 1,330 cm^{-1} are associated with the $–CH_3$ group. Some bands in the region located at 2,930, 2,856 and 1,472 cm^{-1} are attributed to the $–CH_2$ stretching frequencies, the presence of methylene group. FTIR spectra of pure COPUs and (COPUs-C30B) nanocomposites show a small broad band in the range 4,000–3,500 cm^{-1} which is associated with O–H stretching vibrations hydroxyl ended compounds [29]. Characteristic peaks of hydrogen bonded –NH groups of urethane linkages were observed at 3,325–3,390 cm^{-1} and a small band, seen at 3,420 cm^{-1} is characteristic of stretching of unbound –NH groups. The free urethane carbonyl (C=O) is seen at 1,705 cm^{1} while the peak at 1,670 cm^{-1} is due to hydrogen bonded carbonyl. The small peaks at 2,265 cm^{-1} correspond to the –NCO stretching [33]. When COPUs compared with COPUs-C30B nanocomposites, Small bands at 1,020–1,050 cm^{-1} relate to the stretching vibrations of Si–O–Si from organoclay were seen only in the spectrum of COPUs-C30B nanocomposites [32], signifying that the polymer chains have intercalated into the gallery of organoclay [34].

When COPUs compared with COPUs-C30B nanocomposites (Fig. 3), presence of small bands at 1,560–1,680 cm^{-1} was observed, which is related to the stretching vibrations of hydrogen bonded organoclay were seen in the spectrum of COPUs-C30B nanocomposites, signifying that the polymer chains have intercalated into the galleries of organoclay and formulation of hydrogen bonding more than COPUs due to the COPUs molecules can be grafted onto the organically modified clay surface through the reaction between the –NCO groups and the –OH groups on the organically modified clay. The tethered organoclay may interfere with the H-bond formation in COPUs composites [25, 29].

Isocyanate peaks usually appeared at 2,278 cm^{-1} [31], but Fig. 3 shows no peaks indicating a complete consumption of isocyanate during a reaction between isocyanate and hydroxyl groups existent in the polyols and the organoclay as in COPUs and COPUs-C30B, respectively [25].

In order to investigate the presence of hydrogen bonding in the polymer matrix, the FTIR spectra (Fig. 4) were studied at a wavelength ranges from 1,250 to 1,800 cm^{-1}. The vibrations related to hydrogen bonding were observed at a range of 1,560–1,680 cm^{-1}, found more intense with the increasing percentage of organoclay in the nanocomposites (COPUs-C30B), as compared to neat COPUs [35]. The presence of carbonyl (urethane C=O) was also observed at vibration ranges from 1,721 to 1,731 cm^{-1}, which is may be due to the urethanes part of the polymer matrix [36]. Furthermore, organoclay (Cloisite 30B) has OH groups on its surface and according to the hypothesis of Lee et al. [37] they might interact with –NCO groups of the diisocyanate [38]. Thus, the grafted clay may act as a shield which prevents the formation of hydrogen bonds between urethane (–NHCOO) groups.

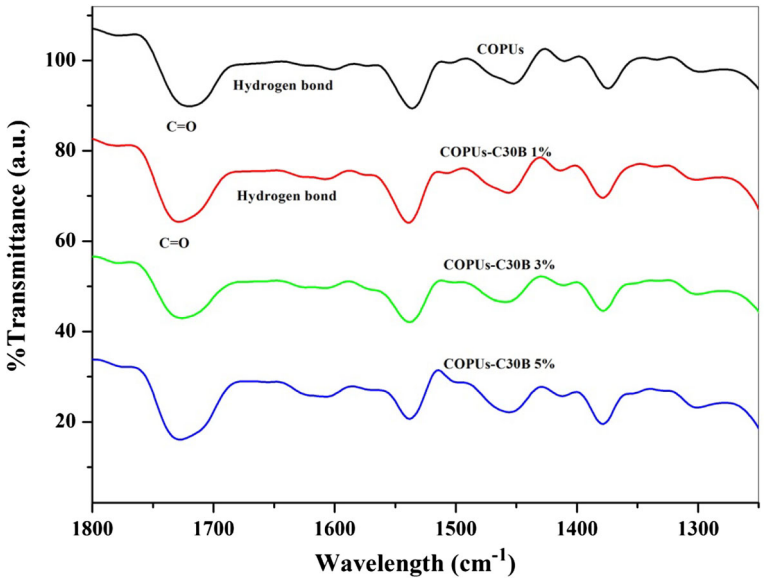

Fig. 4 Comparative FTIR spectra of neat COPUs and (COPUs-C30B) nanocomposites (1, 3, and 5 %) organoclays, with a wavelength range of 1,250–1,800 cm^{-1}

XRD analysis of polyurethane nanocomposites

X-ray diffraction (XRD) was done on organoclay (Cloisite 30B) neat, COPUs and COPUs-C30B composites in order to specify the degree of dispersion of the organoclay particles in the polymer matrix. The (0 0 1) characteristic peak tends to shift to lower angle regime due to expansion of the basal spacing [39]. Figure 5 shows the XRD pattern for chain extended polyurethanes and its polyurethanes clay nanocomposites with varying organoclay content. For organoclay (Cloisite 30B) neat, the (0 0 1) diffraction peak is visible at 5.27, referring to a basal spacing of 16.76 Å; however, this peak is absent in nanocomposite samples.

The shift of the diffraction peak from the (001) plane of Cloisite 30B to lower values that occurs in all of the COPUs-C30B nanocomposites, indicates an increase in the interlayer spacing. In Fig. 5, five diffraction peaks located at $2\theta = 5.27$, 20.59, 20.25, 19.97, and 19.07, corresponding to d spacings of 16.76, 4.311, 4.382, 4.440, and 4.650 Å, respectively, the result refers to organoclay (Cloisite 30B), polyurethane and its polyurethane clay nanocomposites with varying organoclay (Cloisite 30B) content (0, 1, 3 and 5 wt%). It thus appears that the interlayer spacing of the Cloisite 30B in all of the nanocomposites is larger than that in pure Cloisite 30B at the domain of $2\theta = 19$–21, indicating that the polyurethane molecular chains are most likely intercalated and expand into the galleries of silicate layers to form a multilayered structure consisting of layers of polyurethane molecular chains alternating with layers of layered silicate [40, 41].

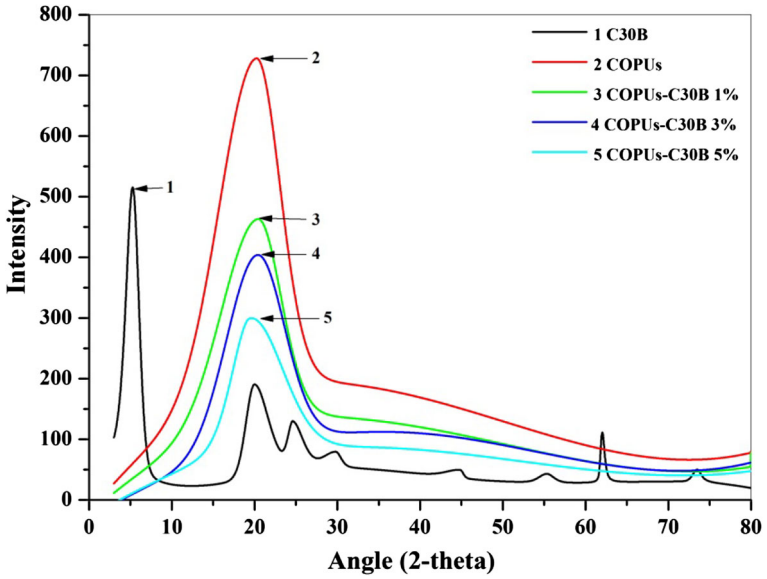

Fig. 5 XRD of organoclay (Cloisite 30B), castor oil-based polyurethanes (COPUs) and COPUs-C30B nanocomposites with varying % of organoclay loading

Field emission scanning electron microscope (FESEM)

The FESEM images of the surfaces of pristine COPUs and the nanocomposites at different weight percentages of 0, 3, and 5 wt% organoclay (Cloisite 30B) are shown in Fig. 6. The pure castor oil based on polyurethanes (COPUs) has a smooth and homogeneous morphology which suggested that a strong interaction existed between the polyurethane chains. These interactions lead to a relatively dense structure without pores or cracks. The homogeneous structures of castor oil-based polyurethanes–organoclay composite (COPUs-C30B) films indicate a high compatibility and miscibility between crosslinked polyurethanes and organoclay [42]. When organoclay content is increased to 5 wt% the morphological structure of the blend films becomes heterogeneous, especially in the case of polyurethanes–organoclays composites. Prepared polyurethanes form dehydrated castor oil showed improved properties due to more crosslinking density by the increases in hydroxyl content [43].

Scanning electron microscopy (SEM)

The micrographs were studied for different (0, 1, 3 and 5) weight % of organoclay as depicted in Fig. 7, where the brighter spots designate the distribution of organoclay particles and the gray colored regions indicate the bulk of the polymer matrix. In castor oil, cell wall formation is found to be slower and larger cells are observed due to the low reactivity of castor oil [44]. The phenomenon of exfoliation, intercalation and aggregation is difficult to study from SEM conclusively, which can

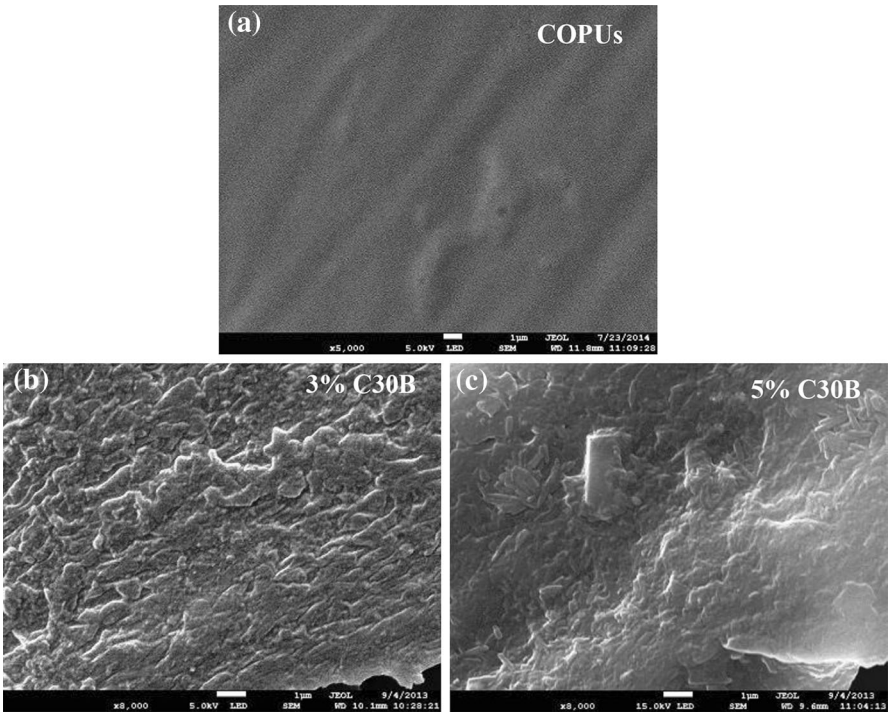

Fig. 6 The FESEM images of the surfaces of pristine COPUs and the nanocomposites at different weight percentages 3, 5 wt% organoclay (Cloisite 30B)

be easily reflected from XRD studies [30]. Figure 7a, with 0 wt% organoclay was smooth and compact, with no evidence of pores. While, Fig. 7b, the surface of COPUs-C30B nanocomposites with 1 weight percentage of organoclay was completely rough, which attributes to the homogeneous distribution of the organoclay aggregate in the polymer matrix. Figure 7c shows micrograph of 3 wt% of organoclay with the best dispersion of the organoclay. SEM images of COPUs-C30B nanocomposite containing 5 % organoclay are shown in Fig. 7d, which shows higher ratio of agglomerates. The nanocomposites were subjected to sonication and high shear mixing. This could be attributed to the chemical interactions between the polar clay surface and polar urethane bonds present in the segments of the polyurethane. There are two types of interactions between the COPUs matrix and layered silicates, hydrogen bonding and chemical bonding [40]. Higher crosslinking density was observed due to an increase in hydroxyl content [43], resulting in improved properties of COPUs nanocomposites.

Thermogravimetric analysis (TGA)

A thermogravimetric study of pure COPUs and clay–polyurethane nanocomposites (different percentages of clay) shown in Fig. 8, depicts two-stage degradation; the

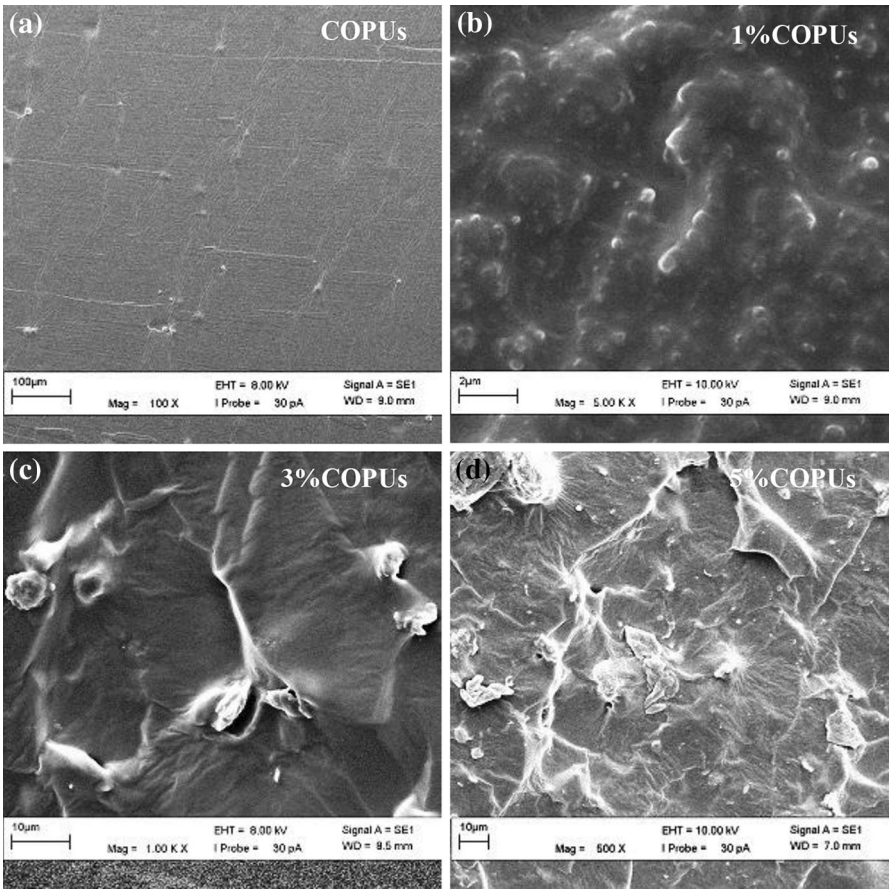

Fig. 7 SEM micrographs image for neat COPUs (**a**) COPUs-C30B nanocomposite with 1 wt% organoclay (Cloisite 30B) (**b**), COPUs-C30B nanocomposite with 3 wt% (**c**) and COPUs-C30B nanocomposite with 5 wt% (**d**)

first stage is mainly governed by the degradation of the hard segment and the second stage connects well with the degradation of the soft segment [45–47], some of them more pronounced than the others. The decomposition temperature of PUs is influenced by the chemical structure of the component having the lowest bond energy [47].

TGA thermograms of the nanocomposites were observed to move toward higher temperatures as compared to neat PUs, indicating the improved thermal stability of the system by the presence of the well-dispersed and exfoliated silicate layers of clay. The polymer–clay nanocomposites exhibit extremely large interface polymers due to the confinement of polymer chains within the galleries of clay platelets of large surface area per unit volume. Nanocomposites show the same TGA profiles as pure polyurethane but displaced to a temperature range 10–30 °C higher than that in the case of the pure PU, which is may be due to

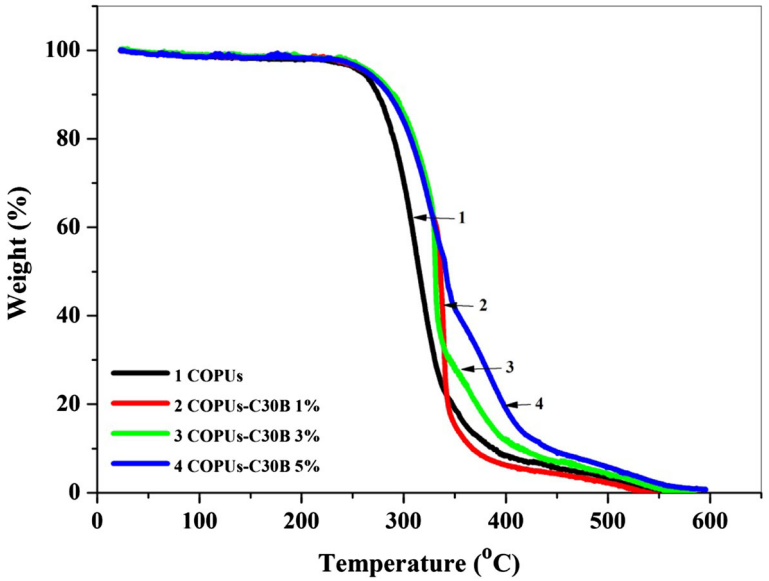

Fig. 8 TGA spectrum of castor oil based on polyurethanes pure and (COPUs) with changing wt% of organoclay (Cloisite 30B) nanocomposite

strong interfacial interaction between the organic clay and PU matrix. The percentage of residue increases from ~6.5 to 12.5 % at 600 °C as the clay contents increased from 0 to 5 wt%, respectively. The first TGA peak is attributed to the overlapping of urethane bond degradation and char-forming secondary reactions (e.g. dimerization, trimerization, crosslinking). At this temperature, breaking of low energy urethane bonding releases CO, CO_2, amines, and aldehydes, whereas the second and third peaks at around 360–380 and 480 °C and above, correspond to decomposition of the stabilized urea/isocyanurate structures, i.e. they are related to the breaking of high-energy bonds, such as C–C, C–O, C–H, C=C, and C=O [48].

Mechanical properties of COPUs-C30B nanocomposites film

Characteristic stress–strain diagrams of polyurethanes based on castor oil (COPUs) and polyurethanes–organoclay nanocomposites of three varying amounts of organoclay. Figures 9 and 10 showed a higher improvement of tensile strength and modulus increased with increased weight percentages of organoclay for all three organoclay loadings in composites of COPUs and TDI. The nanocomposite containing 5 wt% organoclay depicted an improvement of ~240 % in tensile strength and decrease of ~30 % in elongation time, respectively [49]. The improved tensile strength of the system may be due to the presence of the well-dispersed and exfoliated silicate layers of organoclay [50].

The sonication assisted in breaking the clay aggregate [51] into dispersed clay particles. High shear homogenization is beneficial for dispersing the clay platelets

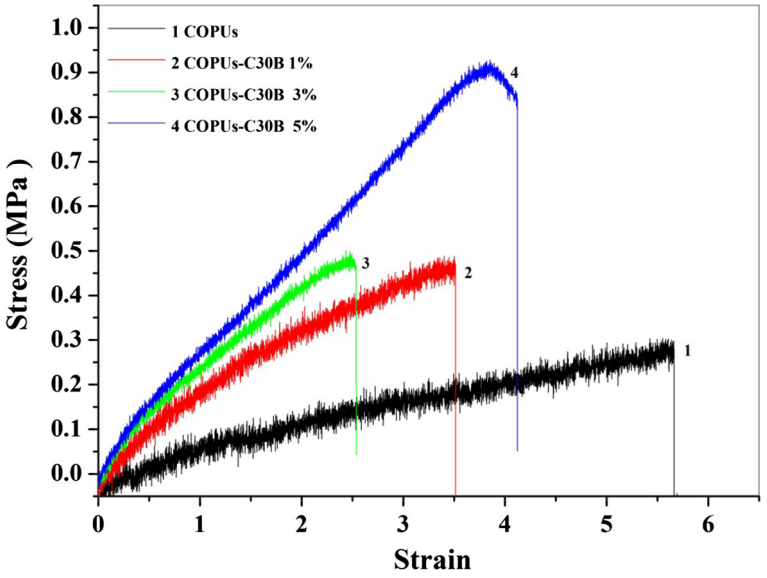

Fig. 9 Stress-strain curves for pure COPUs and COPUs-C30B nanocomposites with varying wt%

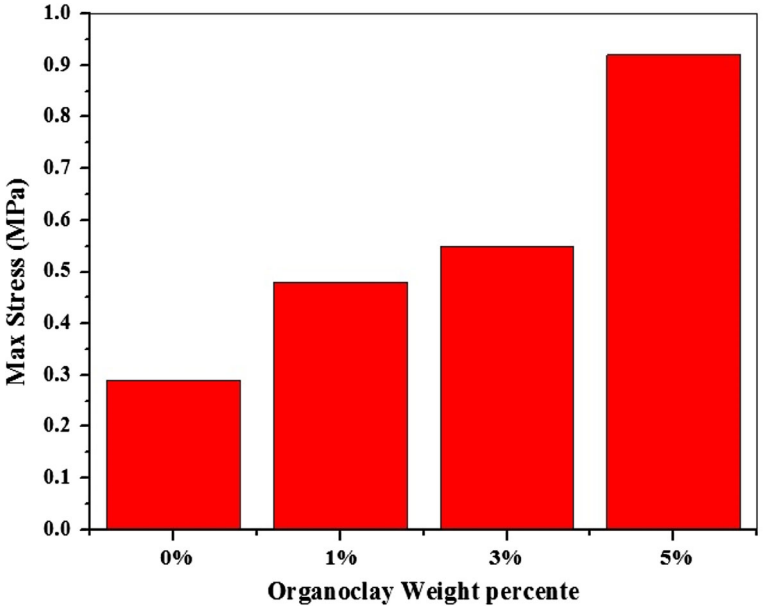

Fig. 10 Tensile strength of COPUs and COPUs-C30B nanocomposites with 0, 1, 3, and 5 wt%

homogeneously [52] throughout the polymer matrix. The main reason for this improvement can be attributed to clay–polymer tethering as well as hydrogen bonding between clay particles and the polymer [42, 53]. Based on the overall

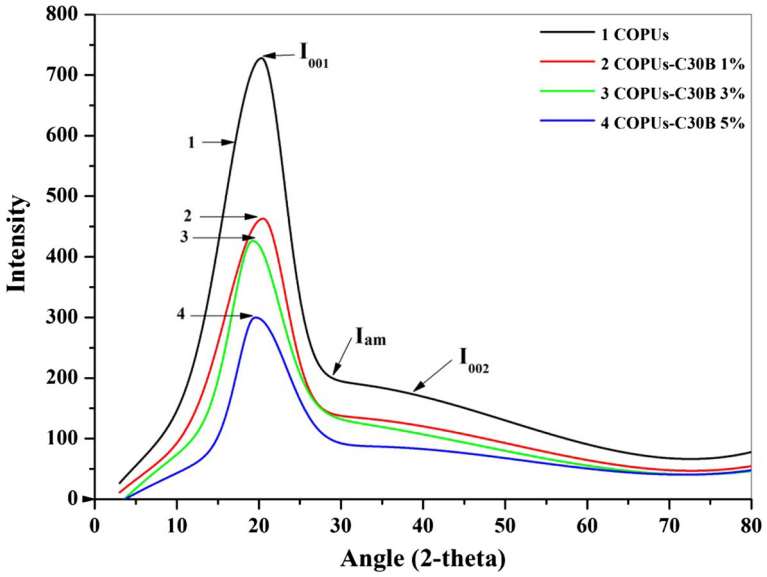

Fig. 11 Depicts the typical example of pure COPUs and COPUs-C30B nanocomposites with different clay wt% crystallinity patterns

Table 1 Crystallinity index of neat COPUs and COPUs-C30B nanocomposites

Sample	I_{001}	2θ	I_{am}	2θ	Cr. I %
COPUs	727.1	20.34	206	28.5	71.7
COPUs-C30B 1 %	463.6	20.49	141	29.44	69.6
COPUs-C30B 3 %	425	19.35	135	29.44	68.2
COPUs-C30B 5 %	300	19.64	97	29.44	67.7

result, the conclusion is that the increased tensility at rupture, which is also associated with the decreased elongation, results in increase of elastic modulus of the polymer, and consequent increase of crosslinking density level.

Percentage of crystallinity

The peaks of neat COPUs and COPUs-C30B nanocomposites (Fig. 11) do not show any significant shift as the organoclay content increases. It implies that all matrix PUs nanocomposites have the same crystal structure, and that nanosize clay layers cannot change the crystal structure. With the organoclay loading, the Bragg peaks have become broader and their intensities have decreased. It indicates that the crystallinity of PUs has decreased as the clay weight percentages have increased [54].

In order to investigate the change in degree of crystallization of PUs composites with different amounts of clay, from Fig. 11, the crystallinity index (CrI) was calculated from Eq. (1) as per the method proposed by Monrroy et al. and Nasir et al. [55, 56].

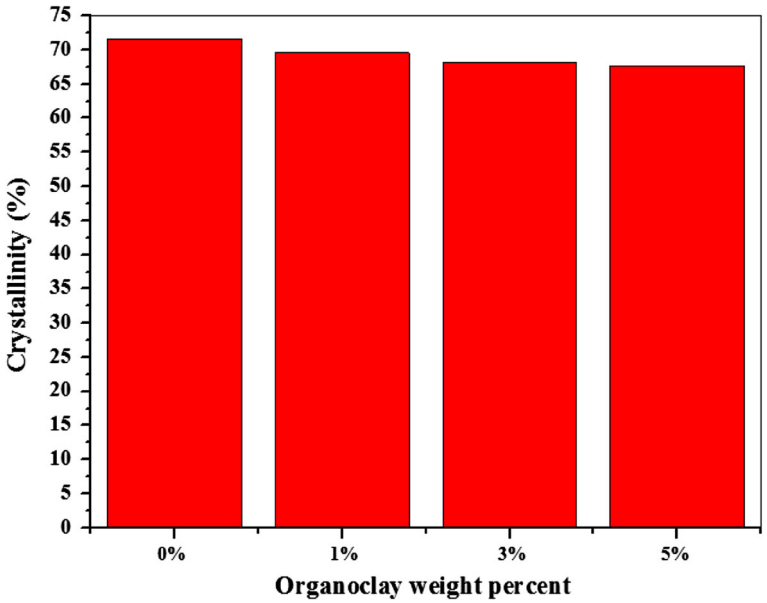

Fig. 12 Crystallinity index (Crl) % pure COPUs and COPUs-C30B nanocomposite at different clay wt%

$$\text{CrI}\ \% = \frac{I_{001} - I_{\text{am}}}{I_{001}} \times 100 \tag{1}$$

where CrI, is crystallinity index of COPUs and COPUs-C30B nanocomposites, I_{001} is intensity of the diffraction peak from the 001 plane around $2\theta = 20.34$, 20.49, 19.35, and 19.64, respectively, while I_{am} is the intensity of the background scatter measured nearly $2\theta = 28.5$ for neat COPUs and $2\theta = 29.44$ for COPUs-C30B nanocomposites, respectively (Fig. 11). The crystallinity index decreased with an increase in the weight percent of organoclay in COPUs composites, as presented in Table 1, and Fig. 12.

The decrease in crystallization of PUs composites due to morphology changes after dispersed nanosize clay layers disrupts the ordered structure of polyurethanes reduction crystallinity index of the soft segment in polyurethane–clay composites as a result of this could be explained by the transformation of the crystalline of PUs into low crystallinity phase inserted into the layer clay galleries. Furthermore, the interaction between the adsorbed PUs chain and the polar groups on the surface layers of clay has prevented the PUs crystallization [41].

Conclusion

In the conclusion, the castor oil-based polyurethanes–organoclay (COPUs-C30B) nanocomposites were synthesized with different (maximum 5 wt%) of organoclay, above which good dispersion became practically impossible. The results of TGA

and FTIR of the nanocomposites, experiments indicated an interaction between the organoclay with polymer matrix improving thermal stability. The morphological appearance of the composite was smooth and uniform in size, with no TDI particles on the surface referring to the perfect interaction. XRD results revealed broad peaks with lower intensity in relation with pure COPUs, which inferred that the organoclay considerably affect the exfoliation and interaction of organoclay with in polymer matrix. Crystallization percentage was found to decrease with increasing percentage of nanofiller in the COPUs matrix. The tensile strength and modulus of the COPUs matrix were significantly enhanced, due to the presence of organoclay and hydrogen bonds crosslinking; formed between ester groups of the COPUs chains and hydroxyl groups on the nanofiller surfaces.

Acknowledgments The authors are thankful for financial support (Research Grant: RDU 130329) from University Malaysia Pahang.

References

1. Stefan O (2013) Effects of guar gum content on structure and properties of multi-crosslinked polyurethane composite films. J Compos Elsevier 44:76–83
2. Yusoh K, Jin J, Song M (2010) Subsurface mechanical properties of polyurethane/organoclay nanocomposite thin films studied by nanoindentation. J Prog Org Coat Elsevier 67:220–224
3. Akintayo CO, Akintayo ET, Ziegler T, Babalola BM (2013) Newly developed epoxy-polyol and epoxy-polyurethane from renewable resources. Br J Appl Sci Technol 3:984–993
4. Nihal S, Emel O (2007) Thermal characteristics of polyurethane foams incorporated with phase change materials. J Thermochim Acta Sci Direct 454:90–98
5. Judit EP, Elizabeth AF, Goy TL, Sara EP, Michelle ME, Steven PS, Marta P, Miros F, Piotr P, Krystal L (2010) A nanostructured carbon-reinforced polyisobutylene-based thermoplastic elastomer. J Biomater Sci Direct 31:2477–2488
6. Bela PJ, Kristof B, Zsuzsa T, Jozsef V, Lajos B, Stephan H, Tamas D, Bela P (2008) Nanophase separation in segmented polyurethane elastomers: effect of specific interactions on structure and properties. J Eur Polym Sci Direct 44:2431–2438
7. Jose MH, Eva M, John CL, Steven SC (2009) Transport properties in polyurethane/clay nanocomposites as barrier materials: effect of processing conditions. J Membr Sci 337:208–214
8. Sponton M, Casisa N, Mazo P, Raud B, Simonetta A, Rios L, Estenoz D (2013) Biodegradation study by Pseudomonas sp. of flexible polyurethane foams derived from castor oil. J Int Biodeterior Biodegrad 85:85–94
9. Laurent F, Houria K, Mylene S, Olivia G, Christine JD, Vincent L, Jean JR (2013) The use of renewable feedstock in UV-curable materials—a new age for polymers and green chemistry. J Prog Polym Sci 38:932–962
10. Xiaohua K, Guoguang L, Hong Q, Jonathan MC (2013) Preparation and characterization of high-solid polyurethane coating systems based on vegetable oil derived polyols. J Prog Org Coat 76:1151–1160
11. Shida M, Ping W, Zhiguo S, Songping Z (2014) Vegetable-oil-based polymers as future polymeric biomaterials. J Acta Biomater 10:1692–1704
12. Eid AI, Motawie AM, Sadek EM (2011) Synthesis and characterization of polyurethane coatings based on soybean oil–polyester polyols. J Egypt J Pet 20:1–8
13. Hadi B, Hamid Y, Shahram MA, Mohammad AS, Seyyed NE (2013) Synthesis and characterization of antibacterial polyurethane coatings from quaternary ammonium salts functionalized soybean oil based polyols. J Mater Sci Eng 33:153–164
14. Hamid Y, Pejman HT (2006) Preparation and properties of novel biodegradable polyurethane networks based on castor oil and poly (ethylene glycol). J Polym Degrad Stabil 92:480–489

15. Ivan S.R, Zoran D.B, Berta H, Katalin M.S, Jaroslava B.S, Nada L, Miodrag K (2012) Thermal stability of polyurethane materials based on castor oil as polyol component. J Therm Anal Calorim. doi:10.1007/s10973-012-2497-x
16. Xiaohua K, Guoguang L, Jonathan MC (2011) Characterization of canola oil based polyurethane wood adhesives. Int J Adhes Adhes 31:559–564
17. Xiaohua K, Guoguang L, Jonathan MC (2012) Novel polyurethane produced from canola oil based poly (ether ester) polyols: synthesis characterization and properties. Eur Polym J 48:2097–2106
18. Guan ST, Takashi N, Hyoe H, Tatsuko H (2011) Polyurethane composites derived from glycerol and molasses polyols filled with oil palm empty fruit bunches studied by TG and DMA. J Thermochim Acta 525:190–196
19. Khoon PA, Choy SL, Sit FC, Cheng HC (2013) Synthesis of palm oil-based polyester polyol for polyurethane adhesive production. J Appl Polym Sci. doi:10.1002/app.39967
20. Hatice M, Michael AR (2010) Castor oil as renewable resource for the chemical industry. Eur J Lipid Sci Technol 112:10–30
21. Corcuera MA, Rueda L, Fernandez BA, Arbelaiz A, Marieta C, Mondragon I, Eceiza A (2010) Microstructure and properties of polyurethanes derived from castor oil. J Polym Degrad Stabil 95:2175–2184
22. Eleni P, Milena GM, Stephen C (2008) Reaction kinetic of polyurethane formation using a comercial oligomeric diisocyanate resin studied by calorimetric and rheological methods. J Macromol Chem Phys 209:2302–2311
23. Hablot E, Zheng D, Bouquey M, Averous L (2008) Polyurethanes based on castor oil: kinetics, chemical, mechanical and thermal properties. J Macromol Mater Eng Polym Sci Technol Gen 293:922–929
24. Ayesha K, Sonia Z, Muhammad IS (2013) High performance segmented polyurethanes derived from a new aromatic diisocyanate and polyol. J Polym Degrad Stabil 98:368–376
25. Caoa X, Lee LJ, Widyab T, Macosko C (2005) Polyurethane/clay nanocomposites foams: processing, structure and properties. J Polym 46:775–783
26. Ling Z (2008) Structure-property relationship of polyurethane flexible foam made from natural oil polyols, PhD Thesis. Doctor of philosophy in chemical engineering and material science, University of Minnesota
27. Thouzeau C, Henneuse C, Sclavons M, Devaux J, Soulestin J, Stoclet G (2013) Emission of volatile organic compounds during processing and use of organoclay based nanocomposites. J Polym Degrad Stabil 98:557–565
28. Gautam D, Ranjan DK, Harekrishna D, Alok KB, Niranjan K (2013) Biodegradation, cytocompatability and performance studies of vegetable oil based hyperbranched polyurethane modified biocompatible sulfonated epoxy resin/clay nanocomposites. J Prog Org Coat 76:1103–1111
29. Kaushik A, Dheeraj A, Vipin S (2011) Synthesis and characterization of organically modified clay/castor oil based chain extended polyurethane nanocomposites. J Compos 42:1534–1541
30. Krushna CP, Nayak PL (2012) Synthesis and characterization of polyurethane nanocomposite from castor oil-hexamethylene diisocyanate (HMDI). J Pelagia Res Libr Adv Appl Sci Res 5:3045–3052
31. Swagatika M, Nayak PL, Guru B, Nanda CP (2010) Synthesis and characterization of polyurethane nanocomposites for biomedical applications, International Conference on Environment. J Energy Dev (from Stockholm to Copenhagen and beyond) 2:403–412
32. dos Santos DJ, Tavares LB, Batalha GF (2012) Mechanical and physical properties investigation of polyurethane material obtained from renewable natural source. J Achiev Mater Manuf Eng 54:211–217
33. Jose M, Cervantes U, Juan V, Cauich R, Humberto VT, Luis F, Garfias M, Donald RP (2009) Thermal degradation of commercially available organoclays studied by TGA-FTIR. J Polym Degrad Stabil 457:92–102
34. Cervantes U, Cauich RJ, Vzquez TH, Garfias ML, Paul DR (2007) Thermal degradation of commercially available organoclays studied by TGA-FTIR. J Thermochim Acta 457:92–102
35. Saha C, Chaki TK, Singha NK (2013) Synthesis and characterization of elastomeric polyurethane and PU/clay nanocomposites based on an aliphatic diisocyanate. J Appl Polym Sci. doi:10.1002/APP.39534 (1–7)
36. Mohanty D, Biswal SK, Palve YP, Nayak PL (2012) Synthesis and characterization of polylactic acid/cloisite 30B (MMT) nanocomposite for controlled release of anticancer drug curcumin. Int J Pharm Res Allied Sci 1(4):63–70

37. Lee LJ, Zeng C, Cao X, Han X, Shen J, Xu G (2005) Polymer nanocomposite foams. J Compos Sci Technol 65:2344–2363
38. Semenzato S, Lorenzetti A, Modesti M, Ugel E, Hrelja D, Besco S, Michelin RA, Sassi A, Facchin G, Zorzi F, Bertan R (2009) A novel phosphorus polyurethane foam/montmorillonite nanocomposite: preparation, characterization and thermal behavior. J Appl Clay Sci 44:35–42
39. Tjong SC (2006) Structural and mechanical properties of polymer nanocomposites. J Mater Sci Eng 53:173–197
40. Dimitry OIH, Ibrahim ZA, Ismail EA, Saad LG (2010) Preparation and properties of elastomeric polyurethane/organically modified montmorillonite nanocomposites. J Polym Res 17:801–813
41. Thuc CN, Cao HT, Nguyen DM, Tran MA, Duclaux L, Grillet AC, Thuc HH (2014) Preparation and characterization of polyurethane nanocomposites using vietnamese montmorillonite modified by polyol surfactants. J Nanomater. ID 302735, 1–11
42. Zhong BX, Wei WK, Ming XZ, Mao P (2010) Effect of surface modification of montmorillonite on the properties of rigid polyurethane foam composites. Chin J Polym Sci 45:1065–1073
43. Dave VJ, Hasmukh SP (2013) Synthesis and characterization of interpenetrating polymer networks from transesterified castor oil based polyurethane and polystyrene. J Saudi Chem Soc Prod Hosting Elsevier. doi:10.1016/j.jscs.2013.08.001 (1–6)
44. Pratondo E, Adityo WH, Eva ON (2012) Sumarno effects of chain extender to the structure of castor oil-based polyurethane foam. In: Proceeding of International Conference on Chemical and Material Engineering. ISBN: 978-602-097-281-7
45. Leszczynska A, Njugunab J, Pielichowski K, Banerjee JR (2007) Polymer/montmorillonite nanocomposites with improved thermal properties, Part II: thermal stability of montmorillonite nanocomposites based on different polymeric matrixes. J Thermochim Acta 454:1–22
46. Wang TL, Hsieh TH (1997) Effect of polyol structure and molecular weight on the thermal stability of segmented poly (urethane ureas). J Polym Degrad Stabil J Sci Direct 55:95–102
47. Coutinho FMB, Delpech FMC (2000) Degradation profile of films cast from aqueous polyurethane dispersions. J Poly Degrad Stabil Sci Direct 70:49–57
48. Silva GR, Armando SC, Francine BC, Eliane A, Rodrigo LO (2010) Biodegradation of polyurethanes and nanocomposites to non-cytotoxic degradation products. J Polym Degrad Stabil Sci Direct 95:491–499
49. Petrovic ZS (2010) Polymers from biological oils, petrovic, polymers from biological oils contemporary materials. Kansas Polymer Research Center, Pittsburg State University, Pittsburg, Kansas, USA I-1:39–50
50. Chen YW, Lee YK, Chen YT, Wu JC (2007) High improvement in the properties of exfoliated PU/clay nanocomposites by the alternative swelling process. J Polym Sci Direct 48:2969–2979
51. Heidarian M, Shishesaz MR, Kassiriha SM, Nematollahi M (2011) Study on the effect of ultrasonication time on transport properties of polyurethane/organoclay nanocomposite coatings. J Coat Technol 8:265–274
52. Andrea D, Alessandro P, Amabile P (2011) Effect of the polymer–filler interaction on the thermomechanical response of polyurethane–clay nanocomposites from blocked prepolymer. J Reinf Plast Compos 30:325–335
53. Chih WC, Ting KH, Wang YC, Bryan GA, Jiang JL (2013) Intercalation strategies in clay/polymer hybrids. J Prog Polym Sci. Available online 13 July: 1–43
54. Abareshi M, Zebarjad SM, Goharshadi EK (2009) Crystallinity behavior of MDPE-clay nanocomposites fabricated using ball milling method. J Compos Mater 43:2821–2830. doi:10.1177/0021998309345307
55. Monrroy M, Ortega I, Ramírez M, Baeza J, Freer J (2011) Structural change in wood by brown rot fungi and effect on enzymatic hydrolysis. Enzyme Microb J Technol 49(5):472–477
56. Nasir M, Arun G, Mohammad D, Hossen B, Gek KC, Mohd A (2014) Laccase application in medium density fibreboard to prepare a bio-composite. J R Soc Chem 4:11520–11527. doi:10.1039/c3ra40593a